RF Transient Analysis and Stabilization of the Phase and Energy of the Proposed PIP-II LINAC

J. P. Edelen, *Member, IEEE*, and B. E. Chase, *Member, IEEE*

***Abstract*— This paper describes a recent effort to develop and benchmark a simulation tool for the analysis of radio frequency (RF) transients and their compensation in an H-linear accelerator. Existing tools in this area either focus on electron linear accelerators (LINACs) or lack fundamental details about the low level radio frequency system that are necessary to provide realistic performance estimates. In this paper, we begin with a discussion of our computational models followed by benchmarking with existing beam-dynamics codes and measured data. We then analyze the effect of RF transients and their compensation in the Proton Improvement Plan-II LINAC, followed by an analysis of calibration errors and how Newton's method-based feedback scheme can be used to regulate the beam energy to within the specified limits.**

***Index Terms*— Ion accelerators, linear accelerators (LINACs), particle accelerators.**

I. Introduction

IN ORDER to facilitate the next generation of neutrino experiments, Fermilab has proposed an upgrade to the accelerator complex to enable operation with a beam power of 1.2 MW, referred to as the Proton Improvement Plan-II (PIP-II). This upgrade includes the construction of an 800-MeV superconducting H-minus linear accelerator (LINAC) [1]. As part of this upgrade, injection into the booster synchrotron will be handled by longitudinal phase space painting in order to improve the longitudinal stability of the beam. In order for this scheme to perform as desired, the beam generated in the LINAC must have very tight tolerances on the energy spread that is also stable with time. This levies a requirement on the low level radio frequency (LLRF) system to regulate the amplitude and phase of each cavity to better than 0.01° in phase and 0.01% in amplitude. The current state of the art in LLRF control can deliver this level of local regulation [2]; however, this does not compensate for errors in the initial cavity phase and amplitude calibration, the effects of beam-loading transients, or drifts in the system over time. In order to understand how calibration errors, system drifts, and beam-loading transients affect the output energy of the beam, we have developed a simulation code that can be paired with existing accelerator physics codes to give estimates for these effects.

While some tools currently exist to study these effects, there are some shortcomings that make them less useful for the study of the PIP-II accelerator specifically. Berkley Lab has developed a code to analyze the performance of the Linear Coherent Light Source II LLRF system [3]; however, it is strictly for electrons (i.e., assumes that $\beta = 1$) and, therefore, does not handle changes in the beam velocity along the accelerator. TraceWin also has a mechanism for handling the interaction of beam-loading and the LLRF system [4], but it too has some shortcomings that make it difficult to develop a full picture of how the interaction of the LLRF control system and the beam will affect the beam performance. First, the model of the LLRF system in TraceWin does not include any integral feedback gain, which will result in a steady-state offset in the cavity magnitude and phase, and poor disturbance rejection. Additionally, there is no mechanism to apply a feed-forward correction term often used to compensate for beam-loading transients, thus limiting the ability of the code to fully analyze the beam performance.

In order to study these effects in detail, we have developed a tool that calculates the effects of beam-loading disturbances on the LLRF system and then applies the subsequent cavity response to the beam at each cavity along the LINAC. This tool also has the ability to implement feed-forward compensation for transient beam loading and the framework for analyzing beam-based feedback schemes to correct for drift in the LINAC and errors in the initial amplitude and phase calibrations in the LINAC. This paper begins with a discussion of the algorithms used to calculate the effects of radio frequency (RF) transients on the beam energy and phase. Then, we provide an overview of the PIP-II LINAC in order to provide context for the benchmarking simulations and the PIP-II case study. Next, we discuss the code benchmarking and cavity sensitivity studies for the PIP-II LINAC. Following this, we show simulation results for the nominal PIP-II LINAC design with and without feed-forward beam loading compensation. Finally, we analyze control schemes to correct for initial calibration errors and for drift in the LINAC over time.

II. Beam-Dynamics and RF Cavity Model

The simulation calculates single-particle trajectories using the drift-kick method, where each particle represents a bunch

Manuscript received April 23, 2018; revised June 3, 2018; accepted June 16, 2018. Date of publication June 21, 2018; date of current version August 15, 2018. This work was supported by Fermi Research Alliance, LLC, under Grant De-AC02-07CH11359.

J. P. Edelen is with RadiaSoft LLC, Boulder, CO 80301 USA (e-mail: jedelen@radiasoft.net).

B. E. Chase is with the Fermi National Accelerator Laboratory, Batavia, IL 60510 USA.

Color versions of one or more of the figures in this paper are available online at http://ieeexplore.ieee.org.

Digital Object Identifier 10.1109/TNS.2018.2849565

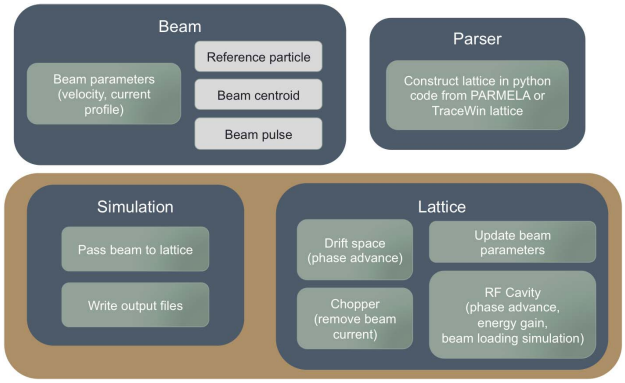

Fig. 1. Block diagram of the overall simulation architecture.

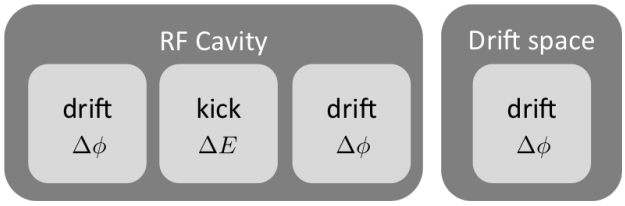

Fig. 2. Block diagram of the beam-dynamics model showing how the cavities are broken down into two drifts and a kick.

in the bunch train. This simplified model allows us to study energy and phase errors for individual bunches due to transients in the RF cavities in an expedient fashion. Additionally, due to the structure of the code, adding in multiparticle tracking for each bunch is feasible. Each simulation is comprised of three basic elements, the simulation engine, the beam, and the lattice. The simulation engine is responsible for passing the beam to each of the lattice elements as well as writing the output files. The beam element contains coordinates for the reference particle, the centroid particle, and the particles in the beam pulse. The lattice contains the beam-line elements, including RF cavities, drift spaces, and a chopper element. The details of the RF cavities and drift spaces are provided in this section, while the chopper element is not discussed in detail. For our code, the chopper element simply serves as a mechanism to reduce the average current. Additionally, we have a parser that translates simulation files from PARMELA [5] and TraceWin into the format for our code. Fig. 1 shows a block diagram of the different simulation elements and their different relationships.

It is convenient to represent the beam and the cavities as complex signals and compute magnitude and phase during the postprocessing. Throughout this paper, complex numbers will be annotated in bold as $\mathbf{x}$, where the magnitude and the phase are given by $|\mathbf{x}|$ and $\angle\mathbf{x}$, respectively.

A. Beam-Dynamics Model

The beam-dynamics model utilizes the drift-kick method. RF cavities are treated as a drift followed by a kick applied at the center of the cavity followed by a second drift. This approximation assumes that the velocity of the beam is not changing in the RF gap and that the energy gain can be computed in the normal way using the peak field, cavity length, and transit time factor [6]. A block diagram of a cavity and a drift is shown in Fig. 2. The kick applied to each particle by the RF cavities is given in

$$\Delta E = |\mathbf{V}_{\text{cav}}(t)| \cos\left(\phi_s + \angle\mathbf{V}_{\text{cav}}(t) + \phi_{\text{beam}}(t) - \phi_r\right) \quad (1)$$

where $\mathbf{V}_{\text{cav}}(t)$ is the cavity voltage as a function of time during the beam pulse, obtained from the RF simulation described in Section II-B, ϕ_s is the design phase of the cavity, $\phi_{\text{beam}}(t)$ is the beam phase as a function of time during the beam pulse, and ϕ_r is the phase of the reference particle. In the simulations, we track the absolute phase of the beam and the reference particle as they transit down the LINAC. For the reference particle, we assume that it arrives at the cavity at the synchronous phase; therefore, its energy gain is $\Delta E_{\text{reference}} = V_{\text{cav}} \cos(\phi_s)$. This convention was chosen to avoid the need to track the individual cavity phases during the simulation. Here, V_{cav} is the peak energy gain for each cavity, which is determined from particle tracking simulations that use the full cavity field map. Note that we do not model any higher order effects due to nonrelativistic beams. Instead, we require the nominal energy gain in our simulation to be identical to the nominal energy gain determined by the beam-dynamics simulations. Put another way to compute V_{cav} for each cavity using the results of detailed beam-dynamics simulations, $V_{\text{cav}} = \Delta E / \cos(\phi_s)$. The phase advance of the drifts is calculated using

$$\Delta\phi(t) = \frac{\omega_0 L}{\beta(t)c} \quad (2)$$

where $\Delta\phi(t)$ is the phase advance as a function of time along the beam pulse, ω_0 is the RF frequency of the proceeding RF cavity, L is the length of drift, and $\beta(t)c$ is the velocity of the beam as a function of time along the beam pulse.

B. RF System Model

The RF control system is modeled using the baseband cavity envelope equation given by [7]

$$\frac{d\mathbf{V}_{\text{cav}}}{dt} = \frac{r/Q\ \omega_0}{4}\mathbf{I}(t) - \frac{\omega_0}{2\ Q_{\text{L}}}\mathbf{V}_{\text{cav}}(t) \quad (3)$$

where $\mathbf{V}_{\text{cav}}$ is the cavity voltage, ω is the RF frequency of the cavity, r/Q is the normalized shunt impedance, and Q_{L} is the loaded quality factor of the cavity. $\mathbf{I}(t)$ represents the total source current given by $\mathbf{I}(t) = \mathbf{I}_{\text{b}}(t) + \mathbf{I}_{\text{ff}}(t) + \mathbf{I}_{\text{drive}}(t)$, where $\mathbf{I}_{\text{b}}(t)$ is the beam current, $\mathbf{I}_{\text{ff}}$ is the feed-forward current, and $\mathbf{I}_{\text{drive}}$ is the drive current. The drive current is used to model the feedback system using

$$\mathbf{I}_{\text{drive}}(t) = \frac{-k_p \mathbf{E}_{\text{cav}}(t - t_{\text{d}})}{R} - k_i \int_0^t \frac{\mathbf{E}_{\text{cav}}(t - t_{\text{d}})}{R} dt \quad (4)$$

where $\mathbf{E}_{\text{cav}} = \mathbf{V}_{\text{cav}} - \mathbf{V}_{\text{set}}$, k_p is the proportional gain, k_i is the integral gain, t_{d} is the group delay of the feedback system, and R is the circuit model resistance designed by $R = (r/Q)Q_{\text{L}}/2$. Note that there is a factor of 2 missing from $\mathbf{I}_{\text{drive}}$ and $\mathbf{I}_{\text{ff}}$; this is due to the fact that the loop gain of the control system is calibrated to be unity. For this calibration, we consider that for an integral gain of 0 and a proportional gain of 1,

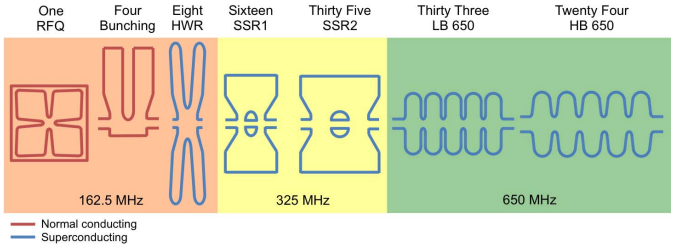

Fig. 3. Cartoon of the PIP-II LINAC cavities arranged as they appear in the accelerator.

the steady-state voltage in the absence of beam loading is $\mathbf{V}_{\text{set}}/2$. Analysis of (3) and (4) under these conditions for our defined current satisfies this condition.

Using (3) and (4), we can solve for the time-domain response of an RF cavity in the presence of beam loading, with a proper LLRF feedback model, and analyze transient compensation through the use of feed forward. Note that while this model does not account for detuning, it is reasonable to expect that the LLRF system in conjunction with the resonance control system is meeting its specification in the absence of beam loading. For future studies, detuning could easily be added to the time-domain simulation if desired. Following this logic, we set the initial cavity voltage equal to the set point $[\mathbf{V}_{\text{cav}}(0) = V_{\text{set}}]$, where V_{set} is the peak energy gain of the cavity determined by the LINAC design simulations and is a real value. Note that while the initial cavity phase is zero, the beam phase is given by the LINAC design, which is used to calculate the complex beam current by $\mathbf{I}_{\text{beam}}(t) = I_{\text{beam}}(t)\cos(\phi_{\text{beam}}(t) - \phi_r + \phi_s) + jI_{\text{beam}}(t)\sin(\phi_{\text{beam}}(t) - \phi_r + \phi_s)$, where $I_{\text{beam}}(t)$ is the real beam current, ϕ_{beam} is the real beam phase, ϕ_r is the reference phase, and ϕ_s is the synchronous phase for the given cavity.

III. Overview of the PIP-II LINAC

Sections IV–VI present results on benchmarking and of case studies using the PIP-II LINAC as a test bench. This section provides an overview of the PIP-II LINAC in order to give some context to Sections IV–VI. The proposed PIP-II LINAC is comprised of seven different types of RF cavities. A room temperature RF quadrupole (RFQ), four room temperature bunching cavities, eight superconducting half-wave resonators (HWRs), 16 type-one superconducting single-spoke resonators (SSR1), 35 type-two superconducting single-spoke resonators (SSR2), 33 low-beta superconducting elliptical cavities (LB650), and 24 high-beta superconducting elliptical cavities (HB650). Due to the complexities of simulating the beam dynamics of an RFQ, we omit those details from this analysis and focus on the cavities downstream of the RFQ. Fig. 3 shows a cartoon of the LINAC cavities as they appear in the accelerator, and Table I shows the parameters used in the RF cavity simulation for each cavity type. The feedback gains were chosen such that all control loops have similar closed-loop bandwidth while reducing the amount of integrator windup at high frequencies.

Fig. 4 gives an overview of the LINAC design for energy gain and acceleration phase; for information regarding the details of the design, the reader should refer to the PIP-II Reference Design Report [1].

TABLE I

Parameters for the Six Types of Cavities in the PIP-II LINAC. Here, Q_L Is the Loaded Quality Factor, r/Q Is the Characteristic Impedance of the Cavities, k_p Is the Proportional Feedback Gain for the LLRF System, and k_i Is the Integral Gain for the Feedback Loop

Type	Frequency	Q_{L}	r/Q	k_p	k_i [1/s]
Buncher	162.5 MHz	4850	530	2.5	3×10^5
HWR	162.5 MHz	2.7×10^6	275	665	4×10^7
SSR1	350 MHz	3.7×10^6	242	455	4×10^7
SSR2	350 MHz	5.2×10^6	296	713	4×10^7
LB650	650 MHz	11.3×10^6	375	695	4×10^7
HB650	650 MHz	11.5×10^6	609	707	4×10^7

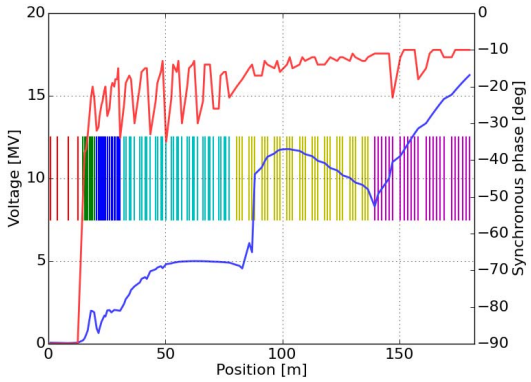

Fig. 4. Energy gain (blue) and synchronous phase (red) as a function of position along the LINAC. Vertical lines: locations of RF cavities. Red lines: bunching cavities. Green lines: HWRs. Blue lines: SSR1s. Cyan lines: SSR2s. Yellow lines: LB650s. Magenta lines: HB650 cavities.

Here, the red vertical lines are the bunching cavities, the green vertical lines are the HWR cavities, the blue vertical lines are the SSR1 cavities, the cyan vertical lines are the SSR2 cavities, the yellow vertical lines are the LB650 cavities, and the magenta vertical lines are the HB650 cavities. The blue plot shows the cavity voltage as a function of position along the LINAC and the red plot shows the synchronous phase as a function of position along the LINAC.

IV. Model Benchmarking

Next, we perform benchmarking studies of our code using a detailed model of the PIP-II LINAC simulated in PARMELA and measured data from the PIP-II Injector Test. The first benchmarking study was focused on the beam dynamics, while the second was focused on the RF transient simulation.

A. Beam-Dynamics Model

Benchmarking of the beam-dynamics model was accomplished by comparing the results of a cavity-phase sensitivity study performed using both PARMELA and our code. For this paper, we calculated the change in energy and phase at the end of the LINAC due to phase perturbations to

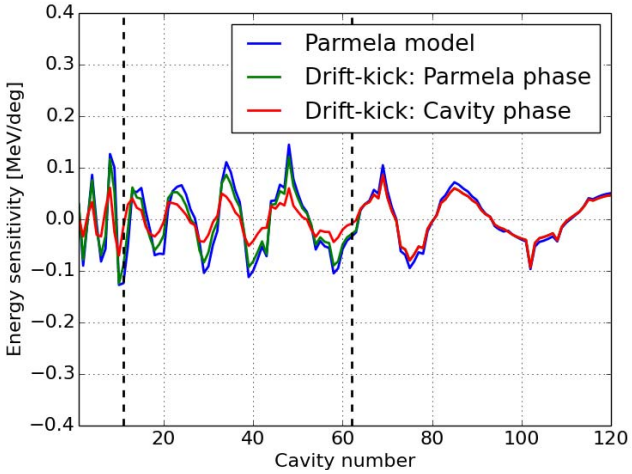

Fig. 5. Energy sensitivity at the end of the LINAC to phase perturbations as a function of the cavity number. The dotted lines indicate where frequency transitions from 162.5 to 325 MHz and from 325 to 650 MHz.

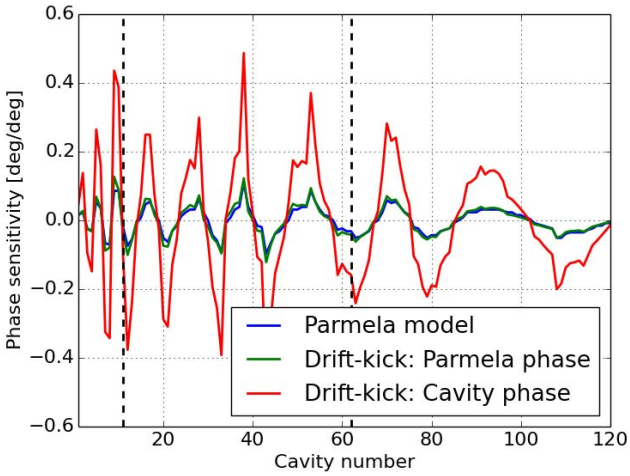

Fig. 6. Phase sensitivity at the end of the LINAC to phase perturbations as a function of cavity number. The dotted lines indicate where frequency transitions from 162.5 to 325 MHz and from 325 to 650 MHz.

individual cavities. Full 3-D cavity field maps were used in the PARMELA simulation. It is important to note that we have chosen a phase convention that differs from that used in PARMELA. PARMELA utilizes a global frequency clock to calculate the beam phase along the LINAC, while the phases of cavities operating at a different frequency are scaled by the ratio of the cavity frequency to the clock frequency. In an operational machine, the beam has no knowledge of this reference frequency and sees each cavity independently. Therefore, we have chosen a phase convention in our code that calculates the phase advance of the drifts based on the frequency of the proceeding cavity. In order to provide an apples-to-apples comparison for benchmarking, we simulated the sensitivity study using both PARMELA's phase convention and our phase convention. Figs. 5 and 6 show the sensitivity of the beam energy and phase at the end of the LINAC, respectively, as a function of cavity number due to small perturbations in the phase of each cavity. Here, we can see

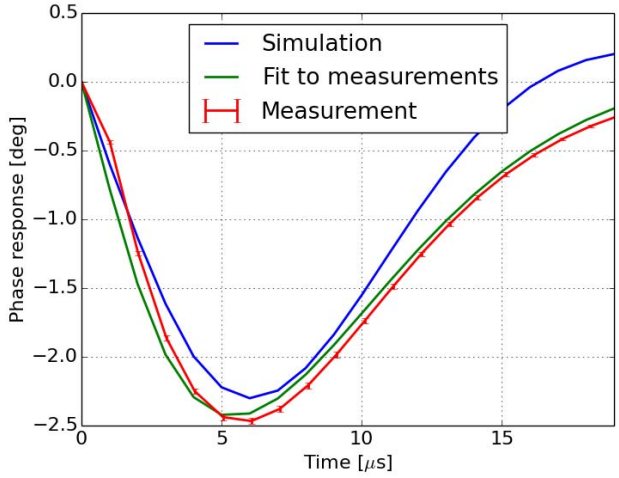

Fig. 7. Comparison of measurement and simulation of a beam loading disturbance in a room temperature bunching cavity. The beam was 20 μs long averaged over 25 pulses.

that when we use the PARMELA phase convention, the drift-kick model and PARMELA agree quite well. However, when we use our phase convention, the drift-kick model does not match the PARMELA model as well especially for phase. This indicates that the drift-kick approximation will provide meaningful results for understanding energy and phase errors in the LINAC and that we should be very cautious about phase conventions in multifrequency LINACs. This paper also provides insight about the sensitivity of different areas of the LINAC. In general, large phase errors result in comparatively small energy errors for individual cavities, and the end of the LINAC is slightly more sensitive than the beginning of the LINAC. Additionally, because we are injecting the bunches into very large RF buckets in the booster, the energy errors are much more important than the phase errors.

B. RF Simulations

The RF simulation can be benchmarked by the comparison of simulation results with measured data from one of the room temperature bunching cavities installed at the PIP-II injector test [8]. Fig. 7 shows the phase response of a bunching cavity due to 5-mA beam disturbance. Q_L for this cavity was measured using a decay and found to be 4850, r/Q is $\approx$530 given by the design documents, and the group delay was assumed to be $\approx$ 2.5 μs (a conservative estimate). Here, we see a relatively good agreement between the model and the measurements. The error bars represent statistical errors in the measurement due to pulse-to-pulse fluctuations in the RF amplifier and noise in the LLRF system. The larger mismatch between the simulation and the measurements can be attributed to systematic errors. Two primary contributors to the mismatch between the model and the measurements are the r/Q value and the group delay. We do not have any measurements of r/Q or of the group delay. Performing a fit of the measurements to the simulations while allowing these two parameters to vary yields the green curve in Fig. 5. The result of this fit is $r/Q \approx 690$ and $t_d \approx 1.72$ μs.

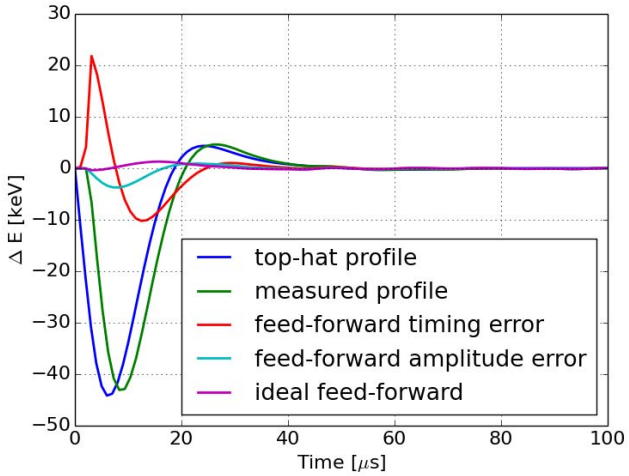

Fig. 8. Modulation in the beam energy at the output of the LINAC due to various beam-loading transient scenarios.

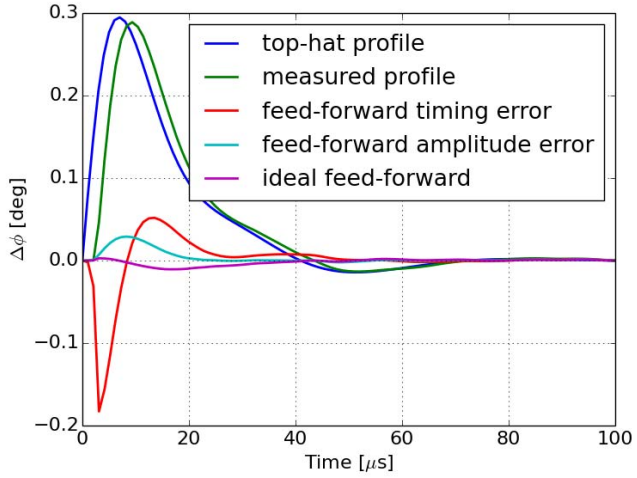

Fig. 9. Modulation in the beam phase at the output of the LINAC due to various beam-loading transient scenarios.

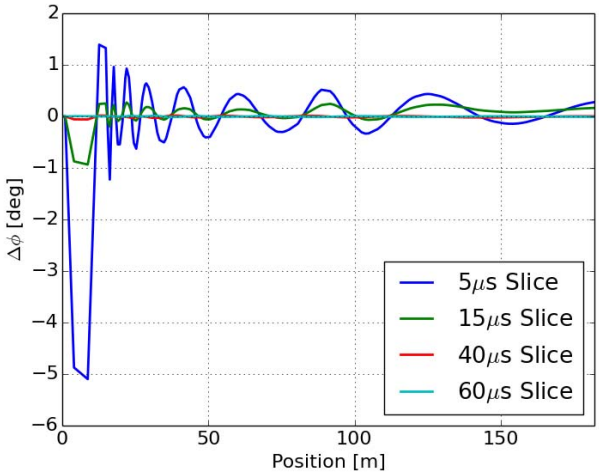

Fig. 10. Deviation from the design phase as a function of position along the LINAC for several slices along the beam.

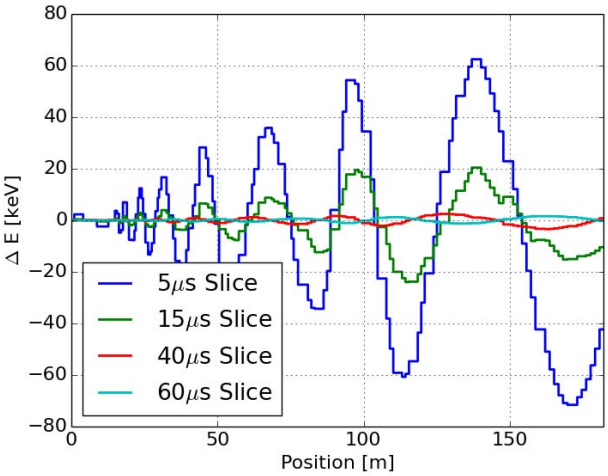

Fig. 11. Deviation from the design energy as a function of position along the LINAC for several slices along the beam.

V. Combined RF and Beam Simulations

With some confidence that our model will provide meaningful estimates of the energy and phase errors induced in the LINAC due to RF cavity transients, we can analyze different beam loading scenarios in the PIP-II LINAC. This is done both for a top-hat beam current distribution and a more realistic beam current distribution taken from measurements in the PIP-II injector test MEBT. Both bunch trains are 500 μs long. The range of cases that can be studied in the LINAC with this code is quite broad. Here, we provide a sample of a few different test cases that illustrate the capabilities of the code and address concerns for meeting performance requirements in the PIP-II LINAC. The first few scenarios show the difference between fully uncompensated transients, partially compensated transients, and fully compensated transients. Figs. 8 and 9 show the energy and phase modulation along the beam pulse, respectively, at the end of the LINAC for these different cases. Here, green and blue show uncompensated transients for the top-hat current distribution and the measured current distribution, respectively, red shows a partially compensated transient using the correct feed-forward current but with a uniform timing error, magenta shows transient compensation that is 90% correct in amplitude and has correct timing, and cyan shows a fully compensated transient. The signal after the first 100μs are not shown because the beam energy and phase are at steady state.

The code also has the ability to look at the evolution of bunches along the bunch train. Figs. 10 and 11 show the large phase errors at the beginning of the LINAC due to high beam loading and long drifts between cavities and small energy errors that increase, as the beam propagates down the LINAC. This is simply because the LINAC has longitudinal focusing, so if the phase deviations damp, the energy deviations must increase.

We can also use the code to analyze errors in the LLRF system, such as faults in the feed-forward compensation, random errors in feed-forward timing and amplitude, and

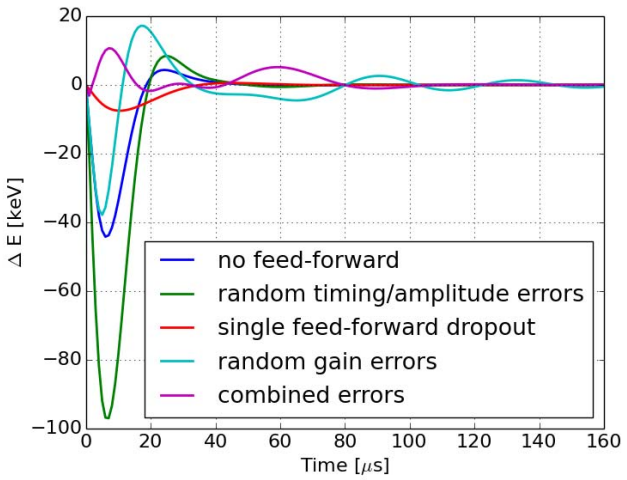

Fig. 12. Modulation in the beam energy at the output of the LINAC due to various errors in the LLRF system.

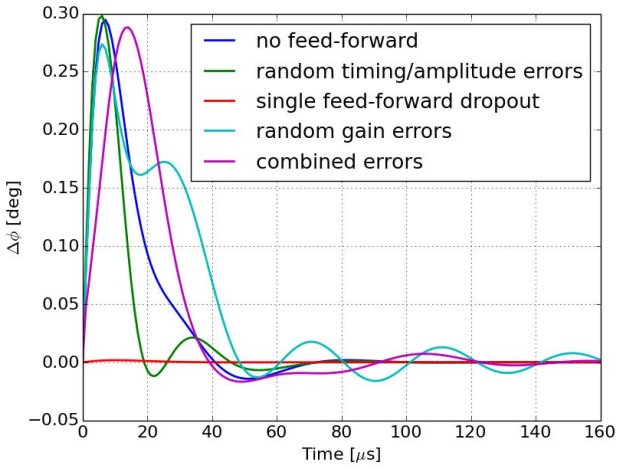

Fig. 13. Modulation in the beam phase at the output of the LINAC due to various errors in the LLRF system.

random errors in the feedback gains. Figs. 12 and 13 show the results of these errors for a top-hat beam current profile.

Here, the blue line shows the energy and phase errors for bunches in the bunch train with no feed-forward compensation and the ideal feedback gains. The green line shows the results of random timing and amplitude errors in the feed-forward compensation for each cavity along the LINAC. The timing errors ranged between 0 and 1 μs and the amplitude errors varied between $\pm 10\%$. Here, we can see that these types of errors can be much more detrimental to the beam profile than no feed-forward compensation. In order to mitigate these effects, each cavity should have a loop to minimize the beam-loading disturbance by adjusting the amplitude and timing of the feed-forward compensation. The red line shows the result of a single cavity feed-forward dropout. The cavity chosen was at the beginning of the LB650 section, which should cause a larger energy error than phase error. Indeed this is what we see and the errors are quite small. It is possible for this code to study these fault scenarios in additional detail; however, that is beyond the scope of this paper. The cyan line shows the result of random gain errors along the LINAC of $\pm 50\%$ without any feed-forward compensation. These gain errors do not have as big of an effect on the peak energy and phase error at the end of the LINAC; however, they do have a significant effect on the phase and energy profile of bunches in the bunch train. Finally, the magenta line shows the effect of these three error studies combined. In general, the most detrimental errors that can occur here are due to feed-forward amplitude and timing errors, which can be easily compensated for by automated feedback in each cavity system. This shows what sort of analysis is feasible using this code and what kind of issues we can expect in the PIP-II LINAC.

VI. Calibration Errors

The analysis in Section V showed how beam-loading transients will impact the beam at the end of the LINAC and how feed forward can be applied to correct for these errors as well as a few fault scenarios. These errors can introduce unwanted modulation of the bunch train energy and phase; however, calibration errors will result in a steady-state offset that can be much larger than the transients observed in Section V. In this section, we study the effect of calibration errors and how to correct them using an online optimization algorithm on the last cryomodule in the LINAC. During commissioning, it is reasonable to expect that we can calibrate each cavity to the proper gradient and phase to within 1% and 0.5°, respectively. This can be accomplished either by the phase scans of the cavities or by the analysis of beam-loading signals with other beam diagnostics [9], [10]. For the PIP-II LINAC, it has been shown that for these levels of calibration errors, the losses in the LINAC are still within acceptable levels [11]. However, these calibration errors are still large enough such that the beam energy error is greater than $10^{-4}\%$. In order to achieve the 10^{-4} energy stability, we propose the use of beam-based feedback using the phase of cavities in the last cryomodule as the control variable to adjust the final beam energy using Newton's Method.

To do this, we first estimate the change in energy due to a change in phase of a cavity given by

$$\frac{dE}{d\phi} = -V_{\text{set}} \sin(\phi_s). \tag{5}$$

We can use (5) in conjunction with Newton's method to determine the phase adjustment of each cavity. This gives the update rule given by

$$\phi_s[n+1] = \phi_s[n] - \frac{E_{\text{error}}}{V_{\text{set}} \sin(\phi_s[n])}. \tag{6}$$

Because we have six cavities in the last cryomodule, the change in phase at each step is scaled by 1/6, as all the cavities have roughly the same relationship between phase and energy gain. The algorithm was then simulated by initializing the lattice with random errors in phase and amplitude for all of the cavities. This was done 10 000 times; in all the cases, the energy converged. The standard error in energy due to random calibration errors of 1% and 0.5° is about 500 keV, while the 4σ error is about 2 MeV. Fig. 14 shows the energy

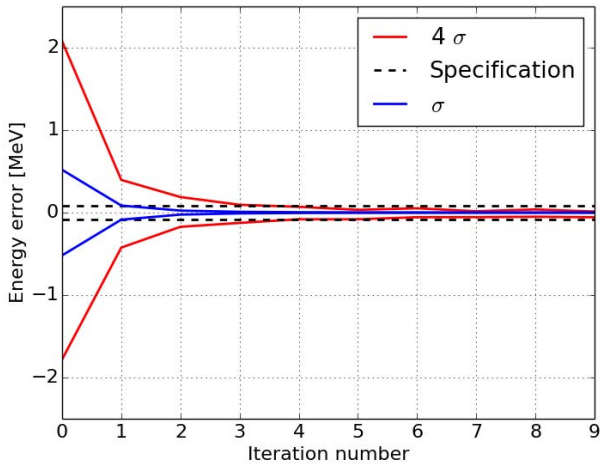

Fig. 14. Beam-based feedback convergence performance.

error as a function of iteration number for the 1σ case and the 4σ case. We can clearly see that in all cases, the energy converges to the desired energy in fewer than five iterations. This gives confidence that we can correct for these calibration errors using beam-based feedback from pulse to pulse and that we can compensate for drift by allowing the algorithm to continuously update the phase settings of the cavities in the last cryomodule.

VII. Conclusion

In this paper, we have shown that the use of a drift-kick beam-dynamics model in conjunction with a complete LLRF feedback model is an efficient method for the analysis of how beam-loading transients impact the beam energy and phase in a pulsed LINAC. We have shown that the beam-dynamics calculations compare well with existing simulation codes and that the RF simulations compare well with the measurements of beam-loading transients. When combined with particle tracking simulations, this presents a means for the study of RF transients and their compensation in a real LINAC. Additionally, we have shown that for the PIP-II LINAC, the use of local feedback with feed-forward compensation for beam-loading transients can stabilize the energy during the pulse at the end of the LINAC to less than ± 5 keV, well within specification. Furthermore, the use of beam-based feedback using the last six cavities can correct for calibration errors and stabilize the energy to the desired value from an initial error of up to 2 MeV. This tool will be quite useful for machine designers and LLRF system designers. It can be used with any particle tracking code given the appropriate parser and is quite versatile for studying a wide variety of fault conditions that could occur in an operational LINAC. The code used for this paper will be made available on request.

References

[1] V. Lebedev. (2015). *The Pip-II Reference Design Report*. [Online]. Available: http://pxie.fnal.gov/PIP-II_CDR/default.htm

[2] J. Branlard, "Low Level RF for SRF Accelerators," in *Proc. 27th Linear Accel. Conf.* Geneva, Switzerland, 2014, pp. 760–764. [Online]. Available: http://jacow.org/LINAC2014/papers/weioa06.pdf

[3] C. Serrano *et al*, "End-to-end FEL beam stability simulation engine," in *Proc. 7th Int. Particle Accel. Conf. (IPAC)*, Busan, South Korea, 2016, pp. 2768–2770. [Online]. Available: http://inspirehep.net/record/1470320/files/wepor043.pdf

[4] J.-L. Biarrotte and D. Uriot, "Dynamic compensation of an rf cavity failure in a superconducting linac," *Phys. Rev. Special Topics-Accel. Beams*, vol. 11, no. 7, p. 072803, 2008.

[5] L. Young and J. Billen, "PARMELA codes," Los Alamos Nat. Lab., New Mexico, NM, USA, Tech. Rep., 2005. [Online]. Available: https://laacg1gov/laacg/services/parmela.html

[6] T. Wangler, *RF Linear Accelerators* (Wiley Series in Beam Physics and Accelerator Technology). Hoboken, NJ, USA: Wiley, 1998. [Online]. Available: https://books.google.com/books?id=9Ho6AQAAIAAJ

[7] T. Schilcher, "Vector sum control of pulsed accelerating fields in Lorentz force detuned superconducting cavities," Ph.D. dissertation, Dept. Phys., Hamburg Univ., Hamburg, Germany, 1998.

[8] G. Romanov *et al.*, "CW room temperature re-buncher for the project X front end," in *Proc. 3rd Int. Conf. Part. Accel. (IPAC)*, New Orleans, LA, USA, May 2012, pp. 3880–3882.

[9] M. Grecki *et al.*, "On-Line RF Amplitude and Phase Calibration," in *Proc. 8th Int. Part. Accel. Conf. (IPAC)*, Copenhagen, Denmark, 2017, pp. 1–3. [Online]. Available: http://inspirehep.net/record/1627345/files/thpab103.pdf

[10] R. Zeng and O. Troeng, "Transient beam loading based calibration for cavity phase and amplitude setting," in *Proc. 57th ICFA* 2016. [Online]. Available: http://inspirehep.net/record/1638759/files/mopl025.pdf

[11] J.-P. Carneiro *et al.*, "Analysis of beam loss mechanism in the project X linac," in *Proc. 24th Part. Accel. Conf. (PAC)*, 2011, pp. 1651–1653. [Online]. Available: http://inspirehep.net/record/896984?ln=en and http://accelconf.web.cern.ch/AccelConf/PAC2011/papers/wep095.pdf